SK4 Ca^{2+} activated K^+ channel is a critical player in cardiac pacemaker derived from human embryonic stem cells

David Weisbrod[a], Asher Peretz[a], Anna Ziskind[b], Nataly Menaker[a], Shimrit Oz[a], Lili Barad[b,c,d], Sivan Eliyahu[b], Joseph Itskovitz-Eldor[b,e], Nathan Dascal[a], Daniel Khananshvili[a], Ofer Binah[b,c,d], and Bernard Attali[a,1]

[a]Department of Physiology and Pharmacology, The Sackler Faculty of Medicine, Tel Aviv University, Ramat Aviv 69978, Israel; [b]The Sohnis Family Stem Cells Center and [c]Department of Physiology of the Ruth and Bruce Rappaport Faculty of Medicine, Technion-Israel Institute of Technology, Haifa 32000, Israel; [e]Department of Obstetrics and Gynecology, Rambam Health Care Campus, Haifa 31096, Israel; and [d]The Rappaport Family Institute for Research in the Medical Sciences, Haifa 31096, Israel

Edited by Richard W. Aldrich, University of Texas at Austin, Austin, TX, and approved March 27, 2013 (received for review December 4, 2012)

Proper expression and function of the cardiac pacemaker is a critical feature of heart physiology. Two main mechanisms have been proposed: (*i*) the "voltage-clock," where the hyperpolarization-activated funny current I_f causes diastolic depolarization that triggers action potential cycling; and (*ii*) the "Ca^{2+} clock," where cyclical release of Ca^{2+} from Ca^{2+} stores depolarizes the membrane during diastole via activation of the Na^+–Ca^{2+} exchanger. Nonetheless, these mechanisms remain controversial. Here, we used human embryonic stem cell-derived cardiomyocytes (hESC-CMs) to study their autonomous beating mechanisms. Combined current- and voltage-clamp recordings from the same cell showed the so-called "voltage and Ca^{2+} clock" pacemaker mechanisms to operate in a mutually exclusive fashion in different cell populations, but also to coexist in other cells. Blocking the "voltage or Ca^{2+} clock" produced a similar depolarization of the maximal diastolic potential (MDP) that culminated by cessation of action potentials, suggesting that they converge to a common pacemaker component. Using patch-clamp recording, real-time PCR, Western blotting, and immunocytochemistry, we identified a previously unrecognized Ca^{2+}-activated intermediate K^+ conductance (IK_{Ca}, KCa3.1, or SK4) in young and old stage-derived hESC-CMs. IK_{Ca} inhibition produced MDP depolarization and pacemaker suppression. By shaping the MDP driving force and exquisitely balancing inward currents during diastolic depolarization, IK_{Ca} appears to play a crucial role in human embryonic cardiac automaticity.

$Ca2^+$-activated K^+ channel SK4 | voltage clock | calcium clock | Na^+-Ca^{2+} exchanger | hyperpolarization-activated cyclic nucleotide-gated channel

Whereas in early embryonic stages all cardiomyocytes are initially endowed with pacemaker activity, during heart development, most cardiac cells will differentiate into working myocardium lacking pacemaker properties. Only a small population of embryonic cardiomyocytes will form the sinoatrial node (SAN), the atrioventricular node, and the bundle of His (1).

A crucial requirement for rhythmic automaticity is the existence of inward currents at diastolic potentials and a subtle dynamic integration of sarcolemmal ion channels, transporters, and Ca^{2+} cycling proteins (2). Various ionic currents finely orchestrate rhythmic automaticity and are referred to as a voltage clock, including the pacemaker or funny current (I_f), L-type, and T-type Ca^{2+} currents (3–10). A Ca^{2+}-dependent pacemaker mechanism referred to as a Ca^{2+} clock was also suggested to be a major player for automaticity, where the rhythmic local Ca^{2+} release from the sarcoplasmic reticulum (SR) drives SAN pacemaker activity. SR Ca^{2+} release via ryanodine receptors (RyRs) is thought to activate the forward mode of the electrogenic sarcolemmal Na^+–Ca^{2+} exchanger (NCX), which generates an inward current contributing to the late diastolic depolarization (DD), before the next action potential (AP) (7, 11). However, the cardiac pacemaker mechanisms remain unclear and controversial (12–15).

Embryonic stem cells differentiate in vitro into spontaneously beating multicellular cardiomyocyte clusters within embryoid bodies (EBs), while recapitulating developmental stages of embryonic cardiomyogenesis (16–27). Thus, human embryonic stem cell-derived cardiomyocytes (hESC-CMs) may provide insights into the pacemaker mechanisms of embryonic cardiac development. In this work, we used the current- and voltage-clamp configurations of the whole-cell patch-clamp technique to record, in the same beating hESC-CM, basal automaticity and ionic currents. This analysis revealed three main pacemaker phenotypes. The first was highly sensitive to I_f current inhibition and insensitive to NCX blockade (28–30). The second cell population exhibited a pacemaker phenotype insensitive to I_f current inhibition, but highly responsive to NCX blockers. The third hESC-CM population displayed pacemaker features that were sensitive to both I_f and NCX blockers, indicating that voltage and Ca^{2+} dependent pacemaker mechanisms can coexist in the same cell. Following exposure to blockers, all three pacemaker phenotypes shared a depolarizing drift of the maximal diastolic potential (MDP) that culminated by cessation of APs, suggesting that they converge to a common pacemaker component, which we identified by patch-clamp recording, real-time PCR, Western blotting, and immunocytochemistry as belonging to the intermediate-conductance Ca^{2+}-activated K^+ channels (IK_{Ca}, KCa3.1 or SK4). Remarkably, IK_{Ca} blockers (31, 32) inhibited the pacemaker in beating hESC-CMs, thereby leading to bradycardia, MDP depolarization, and ultimate suppression of automaticity. The pacemaker activity was sensitive

Significance

The contractions of the heart are initiated and coordinated by pacemaker tissues, responsible for cardiac automaticity. Although the cardiac pacemaker was discovered more than a hundred years ago, the pacemaker mechanisms remain controversial. We used human embryonic stem cell-derived cardiomyocytes to study the embryonic cardiac automaticity of the human heart. We identified a previously unrecognized Ca^{2+}-activated K^+ channel (SK4), which appears to play a pivotal role in cardiac automaticity. Our results suggest that SK4 Ca^{2+}-activated K^+ channels represent an important target for the management of cardiac rhythm disorders and open challenging horizons for developing biological pacemakers.

Author contributions: D.W., A.P., O.B., and B.A. designed research; D.W., A.P., A.Z., N.M., S.O., L.B., and S.E. performed research; A.Z., J.I.-E., N.D., D.K., and O.B. contributed new reagents/analytic tools; D.W., A.P., N.M., and S.O. analyzed data; and B.A. wrote the paper.

The authors declare no conflict of interest.

This article is a PNAS Direct Submission.

[1]To whom correspondence should be addressed. E-mail: battali@post.tau.ac.il.

This article contains supporting information online at www.pnas.org/lookup/suppl/doi:10.1073/pnas.1221022110/-/DCSupplemental.

to IK_{Ca} blockade in 100% of early (EBs 11–21 d in vitro) and in 30% of late (EBs 46–52 d in vitro) stage-derived hESC-CMs. Our results indicate that IK_{Ca} plays a pivotal role in cardiac automaticity by supplying the MDP driving force and by delicately balancing the inward currents of the voltage and Ca^{2+} clocks during diastolic depolarization. KCa3.1 may thus represent an important target for the management of cardiac rhythm disorders.

Results

Heterogeneity of Young Spontaneously Beating hESC-CMs. We used single spontaneously beating hESC-CMs dissociated from young contracting clusters obtained 11–21 d after EBs formation. We recorded alternatively in the same cell spontaneous APs and ionic currents, using, respectively, the current- and voltage-clamp modes of the whole-cell patch-clamp technique. The hESC-CMs were previously found to be heterogeneous in their AP shape, consisting of nodal-like, atrial-like and ventricular-like APs (18, 19, 22, 23, 25). In this study, we also observed different AP shapes (Fig. 1*A*) and found a rather heterogeneous distribution of AP duration at 50% repolarization (APD_{50}) (Fig. 1*B*). A rather weak correlation was found between the APD_{50} length and the AP rate (Fig. 1*C*; r = −0.400, $P < 0.0001$; $n = 100$). Nevertheless, the largest was the APD_{50} value, and the most hyperpolarized was the MDP (Fig. 1*D*; r = −0.491, $P < 0.0001$, $n = 100$). However, we refrained from classifying hESC-CM APs according to mature cardiac phenotype terminology because all recorded cells exhibited pronounced embryonic features with strong pacemaker activity (DD slope = 0.088 ± 0.006 V/s; $n = 78$), very slow upstroke [maximum upstroke velocity (dV/dt_{max}) = 7.09 ± 0.42 V/s; $n = 61$], and depolarized MDP (MDP = −56.5 ± 0.9 mV; n =100). Along this line, there was no correlation between the DD slope and the APD_{50} length (Fig. S1*A*; r = −0.055, $P = 0.628$, $n = 78$). Thus, these young hESC-CMs, much like fetal cardiomyocytes, exhibit automaticity despite different APD_{50} values (33, 34). In agreement with this feature, we found that exposure of hESC-CMs to an external Ca^{2+}-free solution totally suppressed automaticity (Fig. S2*A*; $n = 5$). Also, treatment with the L-type Ca^{2+} channel blocker nifedipine (1 μM) abruptly ceased AP firing (Fig. S2*B*; $n = 5$). In contrast, the pacemaker of these young hESC-CMs was totally insensitive to tetrodotoxin application (10 μM TTX; Fig. S2*C*; $n = 6$). Thus, similar to embryonic cardiomyocytes, the pacemaker activity of these young hESC-CMs entirely depends on external Ca^{2+} influx via L-type Ca^{2+} channels.

Although the I_f current was detected in all tested hESC-CMs, we determined whether it was preferentially expressed in a specific hESC-CMs subpopulation. By recording in the same cells, spontaneous APs and I_f currents, we found no correlation between the I_f current density measured at MDP (a physiologically relevant potential) and APD_{50} values (Fig. S1*B*; r = −0.239, $P = 0.127$, $n = 42$). Similarly, no correlation was found between the I_f current density measured at MDP and the DD slope (Fig. S1*C*; $r = 0.065$, $P = 0.736$, n =29). These data suggest that I_f-dependent and I_f-independent pacemaker mechanisms exist in young hESC-CMs.

hESC-CMs with Prominent I_f-Dependent Pacemaker. Fig. 2*A* shows the spontaneous AP pattern of a hESC-CM. Exposure to the I_f blocker zatebradine (10 μM) nearly suppressed the I_f current as monitored by voltage-clamp in the same cell (Fig. 2 *B* and *C*), markedly reduced the beating rate (Fig. 2 *A* and *D*; 66 ± 4% inhibition, $n = 6$; $P = 0.0035$), and depolarized the MDP (Fig. 2*E*; MDP = −55.4 ± 4.6 mV and MDP = −43.9 ± 5.2 mV before and after zatebradine, respectively; $n = 11$, $P = 0.0058$). The high sensitivity of the pacemaker of these cells to I_f blockade was reflected by the strong reduction of the DD slope following zatebradine exposure (Fig. 2*E*; DD = 0.036 ± 0.008 V/s and DD = 0.013 ± 0.005 V/s before and after zatebradine, respectively; $n = 11$, $P = 0.0078$). Very similar results were obtained when this group of cells was treated with another I_f blocker, ZD7288 (25 μM), which substantially inhibited I_f (Fig. S3*B*) and produced a depolarization drift of the MDP, culminating by cessation of APs (Fig. S3*A*). As shown in Fig. 3, these same cells with a prominent I_f-dependent pacemaker [32% ($n = 19$ out of 58 cells)] were virtually insensitive to two different NCX blockers, 2-(2-[4-(4-nitrobenzyloxy)phenyl] ethyl)isothiourea mesylate (KB-R7943) (3 μM) and the cyclic peptide Phe-Arg-Cys-Arg-Cys-Phe-CONH2 (FRCRCFa) (2 μM) (28–30).

hESC-CMs with Prominent I_f-Independent Pacemaker. In contrast to hESC-CMs exhibiting prominent I_f-dependent pacemaker activity, a different group of cells showed a pacemaker that was practically insensitive to the I_f blockers, zatebradine and ZD7288. As shown in Fig. 4, ZD7288 (25 μM) did not affect the pacemaker activity of this hESC-CM group [41% (n = 24 out of 58 cells)], despite a total suppression of the I_f current (Fig. 4 *A* and *B*). Remarkably, the pacemaker of these same cells was highly sensitive to the NCX blocker KB-R7943 (1–3 μM) in a reversible manner (Fig. 4*C*), causing a decrease in DD slope (Fig. 4*D*; DD = 0.052 ± 0.010 V/s and DD = 0.021 ± 0.008 V/s before and after 1 μM KB-R7943, respectively; $n = 6$, $P = 0.0482$), MDP depolarization (MDP = −57.6 ± 3.8 mV and MDP = −40.5 ± 2.2 mV before and after 1 μM KB-R7943, respectively; $n = 6$, $P = 0.0091$) and ultimately a cessation of APs. To make sure that KB-R7943 did not cross-react with the I_f current, we checked its effect on the I_f current–voltage relation (Fig. S4*A*). Although 25 μM ZD7288 blocked I_f at all voltages (~70% inhibition at −100 mV; $n = 9$), 3 μM KB-R7943 did not affect the I_f current at any voltage (Fig. S4*A*; $n = 3$). Thus, after NCX block, I_f remains intact. In contrast, 3 μM KB-R7943 potently inhibited the NCX current with somewhat better block of outward than inward currents (Fig. S4 *B* and *C*; 61 ± 11% inhibition at −100 mV versus 84 ± 6% inhibition at +50 mV, $n = 6$). In this I_f-independent pacemaker group, zatebradine (10 μM) did not change the AP beating rate, the DD slope, and the MDP (Fig. S5). In contrast, the pacemaker activity of these cells was highly sensitive to another specific NCX blocker (28), the cyclic peptide FRCRCFa, applied in the patch pipette solution (Fig. S6). Within less than 2 min after membrane rupture, FRCRCFa (2 μM)

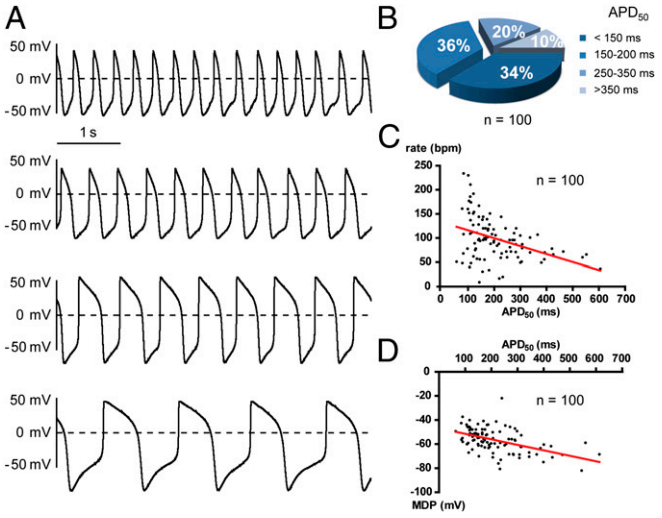

Fig. 1. Heterogeneity of AP morphology in young spontaneously beating hESC-CMs. (*A*) Representative traces of different patterns of spontaneous APs recorded from hESC-CMs. (*B*) Distribution of hESC-CMs based on their APD_{50} ($n = 100$). (*C*) Relation between AP rate and APD_{50} values of hESC-CMs showing a rather weak linear correlation ($P < 0.0001$, r = −0.4006, $n = 100$). (*D*) Relation between MDP and APD_{50} values of hESC-CMs showing a linear correlation ($P < 0.0001$, r = −0.4917, $n = 100$).

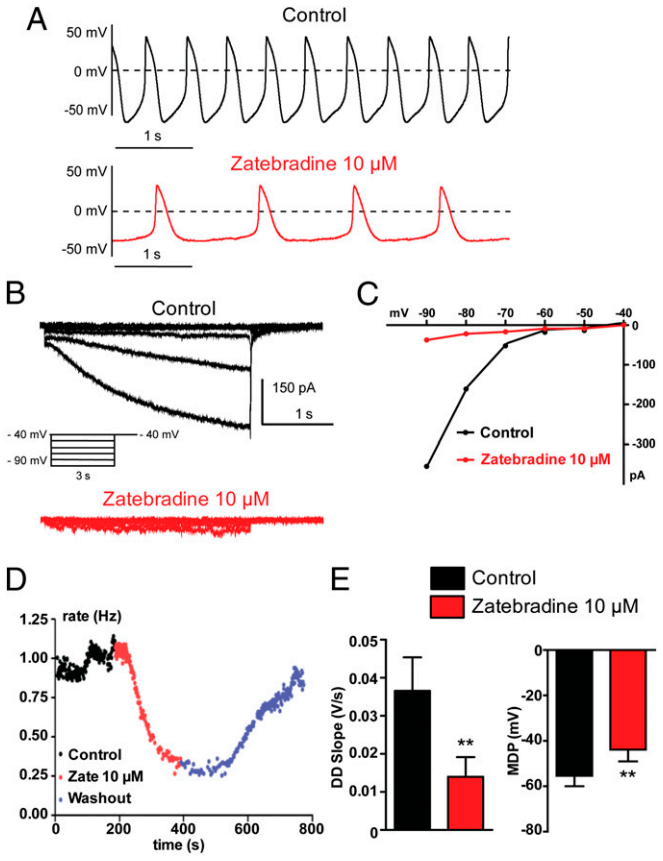

Fig. 2. A subset of hESC-CMs exhibits prominent I_f-dependent pacemaker. (*A–D*) Combined current- and voltage-clamp recordings were performed in the same cell. (*A*, *Upper*) Spontaneous AP pattern of a hESC-CM recorded under current-clamp in control conditions. (*B*) The I_f current was subsequently recorded in the same cell, under voltage-clamp, in the absence (black traces) and presence of 10 μM zatebradine (red traces) by stepping the membrane from a holding potential of −40 mV to −90 mV in 10-mV decrements for 3 s pulse duration. (*C*) Current-voltage relationship of the I_f current from this cell showing the strong inhibitory effect of zatebradine. Once I_f current inhibition by zatebradine was monitored under voltage-clamp, the AP pattern of the same cell was examined under current-clamp, during continuous zatebradine exposure (see *A*, *Lower*). Note the bradycardia and the MDP depolarization. (*D*) Bradycardia was measured over time by the instantaneous frequency between two contiguous APs (in Hz) before (black dots), following 10 μM zatebradine (red dots), and during washout (blue dots). (*E*) Zatebradine (10 μM) significantly decreased the DD slope (**P = 0.0078; n = 11) and depolarized the MDP in this subset of cells (**P = 0.0058; n = 11).

markedly reduced the beating rate (Fig. S6 *A* and *B*; by 79 ± 5%; $n = 6$, $P = 0.0056$) and the DD slope with a pronounced effect on the late DD (Fig. S6*C*; DD = 0.093 ± 0.016 V/s and DD = 0.011 ± 0.003 V/s, immediately after membrane rupture and before cessation of AP, respectively; $n = 12$, $P = 0.0001$). In addition, FRCRCFa (5 μM) depolarized the MDP, which terminated by AP cessation (Fig. S6 *D* and *E*; MDP = −51.5 ± 3.4 mV and MDP = −32.0 ± 5.6 mV, respectively; $n = 5$, $P = 0.0032$). Similarly, isomolar replacement of the external Na^+ solution (140 mM NaCl) by a Li^+ solution (LiCl), which is known to disable NCX function, led to reversible cessation of AP (Fig. S6*F*; $n = 5$). Next, we compared in the voltage-clamp configuration the I_f and NCX current densities in the same cell without knowing a priori whether the hESC-CMs exhibited an I_f-dependent or I_f-independent pacemaker activity. Indeed, the pipet intracellular solution necessary to record the NXC current in isolation (*Materials and Methods*) does not allow the recording of APs in the current-clamp configuration. The results show that, at −50 mV, a voltage value close to the MDP of most recorded hESC-CMs (Fig. 1*D*), the current density of NCX was about threefold larger than that of I_f when recorded in the same cells (Fig. S7; I_{NCX} = −0.76 ± 0.24 pA/pF versus I_f = 0.24 ± 0.09 pA/pF, $n = 5$). At −100 mV, I_f was larger than I_{NCX} (Fig. S7*B*; I_f = -7.30 ± 2.87 pA/pF versus I_{NCX} = −1.96 ± 0.58 pA/pF, respectively; $n = 5$).

hESC-CMs Endowed with both I_f-Dependent and I_f-Independent Pacemakers. A third group of hESC-CMs exhibited an intermediate sensitivity to both I_f and NCX blockers [26% (n = 15 out of 58 cells)]. Fig. S8 shows an example of such a cell where, following exposure to ZD7288 (25 μM), the I_f current was completely suppressed, leading to a substantial but not complete reduction of AP beating accompanied by a diminution of the DD slope with a decrease of the notch at the early DD and a depolarization of the MDP (Fig. S8 *A*, *B*, and *D*). Washout and subsequent addition of 3 μM KB-R7943 also decreased the DD slope and caused MDP depolarization (Fig. S8*C*), culminating in cessation of APs. With respect to inhibition of AP beating rate, three pacemaker phenotypes could be distinguished based on their sensitivity to I_f or NCX blockade: hESC-CMs highly (50–100% inhibition), moderately (25–50% inhibition), and weakly (0–25% inhibition) sensitive to zatebradine (I_f) or FRCRCFa (NCX) (Fig. S8*E*).

Sensitivity of hESC-CM's Pacemaker to Ryanodine Receptor Blockers. Ca^{2+}-cycling proteins such as the RyR thought to activate the forward mode of NCX were suggested to support the Ca^{2+} clock pacemaker mechanism (15, 35, 36). Fig. S9 shows that 1 μM ryanodine initially led to a marked slowing of AP frequency (rate = 94 ± 8 beats per min (bpm) and rate = 36 ± 5 bpm, before and after ryanodine exposure, respectively; n =5, $P = 0.0010$) and reduced the DD slope, mainly at the late phase of the DD, while preserving the notch of the early DD. Subsequently, ryanodine can cause MDP depolarization and ultimately suppression of APs (MDP = −63 ± 3 mV and MDP = −50 ± 4 mV, before and after ryanodine exposure, respectively; n =5, $P = 0.039$). Fig. S9*A* shows that both I_f-dependent (ZD7288-sensitive) and I_f-independent (ZD7288-insensitive) pacemaker hESC-CMs were sensitive to ryanodine.

Identification of a Ca^{2+}-Activated K^+ Current, IK_{Ca}, and Its Impact on Pacemaker Activity. So far, our results revealed that hESC-CMs exhibited three pacemaker phenotypes, one predominantly I_f-dependent, one predominantly I_f-independent, and a combination of both. However, in all cases, these three phenotypes shared a depolarizing drift of the MDP, following exposure to blockers of I_f, NCX, or RyR. These observations suggested to us that inhibition of a putative Ca^{2+}-activated K^+ conductance might be responsible at least partially for this MDP depolarization. Therefore, we hypothesized that such a conductance might constitute a converging new component of the pacemaker mechanism. Large-conductance Ca^{2+}-activated big conductance Ca^{2+}-activated (BK_{Ca}) K^+ channels are not expressed in the sarcolemma of cardiomyocytes (37). However, a recent report suggested that BK_{Ca} channels could play a role in heart rate regulation (38). Thus, we examined the effects of iberiotoxin (100 nM), a selective inhibitor of BK_{Ca} channels, on the pacing of hESC-CMs. Iberiotoxin affected neither the beating rate nor the AP shape of the hESC-CMs (Fig. 5*A*; $n = 3$). Then, we focused our search on small-(SK_{Ca}) and intermediate-(IK_{Ca}) conductance Ca^{2+}-activated K^+ channels. First, we examined under current-clamp the effect of dequalinium, a nonselective blocker of both SK_{Ca} and IK_{Ca} (39). Dequalinium (50 μM) reduced the beating rate and the DD slope and caused MDP depolarization (Fig. 5*B*; MDP = −66.4 ± 4.5 mV and MDP = −49.7 ± 6.1 mV before and after dequalinium exposure, respectively; $n = 5$, $P = 0.0067$). To distinguish between SK_{Ca} and IK_{Ca} channels, we used apamin, a highly selective SK_{Ca} blocker. Apamin at concentrations of up to 1 μM did not affect the AP frequency, APD_{50}, or the DD slope and did not depolarize the

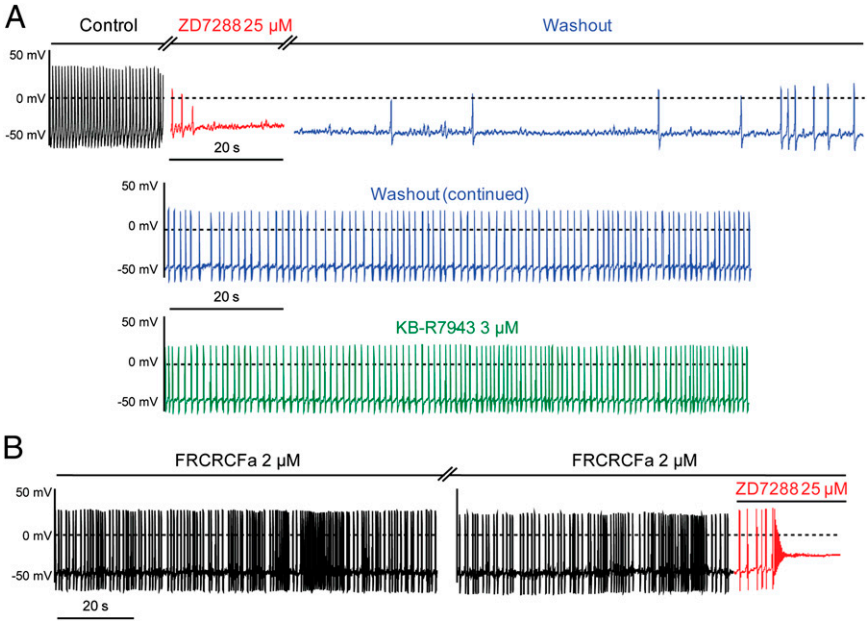

Fig. 3. A subset of hESC-CMs with prominent I_f-dependent pacemaker are sensitive to ZD7288, but insensitive to NCX blockers. (*A*) Spontaneous AP pattern of an hESC-CM recorded under current-clamp in control conditions (black trace, *Top*). The same cell was subsequently exposed to 25 μM ZD7288 (red trace, *Top*), which led to MDP depolarization and cessation of automaticity. Subsequently, ZD7288 was washed out from the same cell (blue trace), which progressively recovered its pacemaker activity (*Middle*). Finally, KB-R7943 (3 μM) was applied to this cell and did not affect automaticity (green trace, *Bottom*). (*B*) Spontaneous AP pattern of an hESC-CM recorded under current-clamp immediately after membrane rupture. The NCX blocker, FRCRCFa (2 μM) was included in the patch pipet. In this type of cell, FRCRCFa was totally inactive on the pacemaker activity; however, when 25 μM ZD7288 (red trace) was added to the bath solution, a very fast MDP depolarization and cessation of automaticity were observed.

MDP (Fig. 5*D*). In contrast, clotrimazole (2 μM), a slightly more selective blocker of IK_{Ca} channels (31, 32), reduced AP beating rate and the DD slope and depolarized MDP until cessation of APs (Fig. 5 *C* and *E*; MDP = −58.8 ± 3.1 mV and MDP = −38.7 ± 5.4 mV before and after clotrimazole exposure, respectively; $n = 5$, $P = 0.0135$). Importantly, clotrimazole did not affect the APD_{50} (Fig. 5*C*). Using a voltage ramp protocol (from −100 mV to +40 mV, with 1 μM free Ca^{2+} in the patch pipet solution), we could isolate a clotrimazole-sensitive current (Fig. 5*F*). We held cells at −20 mV to cause inactivation of nearly all Na^+ channels and a substantial part of Ca^{2+} channels. In the absence of blockers, the voltage ramp (control) revealed the residual presence of a voltage-dependent inward current activating at about −30 mV and corresponding to L-type Ca^{2+} currents as it was eliminated in the presence of 1 μM nifedipine (solution 1). Solution 1, which contained 1 μM nifedipine, 10 μM zatebradine, and 10 μM E4031, an inhibitor of I_{Kr} K^+ current, not only eliminated the inward L-type Ca^{2+} current but also removed a large fraction of an outwardly-rectifying current, yielding a rather linear current trace (Fig. 5*F*, green trace). Addition of 5 μM clotrimazole to solution 1 (+ clotrimazole) symmetrically reduced the linear current trace in both the inward and the outward directions, which under these conditions corresponded to an IK_{Ca} current density of 2.3 ± 0.4 pA/pF ($n = 8$) (Fig. 5*F*, violet trace). This clotrimazole-sensitive current was not detected when the patch pipet solution lacked Ca^{2+}.

To substantiate further the assumption that this clotrimazole-sensitive current corresponds to an IK_{Ca} current, we used 1-[(2-chlorophenyl)diphenylmethyl]-1H-pyrazole (TRAM 34), a specific IK_{Ca} inhibitor (40). TRAM 34 (2 μM) depressed AP beating rate and the DD slope and depolarized MDP until cessation of APs (Fig. 6 *A* and *B*; MDP = −62.7 ± 1.2 mV and MDP = −43.6 ± 1.9 mV before and after TRAM 34 exposure, respectively; $n = 30$, $P =$ 3.16891E−13). Like clotrimazole, TRAM 34 did not affect APD_{50} (Fig. 6*B*). Remarkably, TRAM 34 inhibited the pacemaker activity in all tested cells of the early stage-derived hESC-CMs (EBs 11–21 d in vitro; $n = 30$), including those merely sensitive to I_f blockade and those merely responsive to NCX inhibition (Fig. S10). Next, we characterized TRAM 34-sensitive currents at the single channel level. We used the inside-out configuration of the patch-clamp technique with symmetrical high K^+ solutions containing 1 μM free Ca^{2+}. Stationary recordings from the inside-out patches showed unitary currents that were reversibly sensitive to TRAM 34 blockade (Fig. 6*C*, *Upper*). The unitary current-voltage relations indicated a very mild inward-rectification at depolarized potentials and yielded upon linear regression a unitary slope conductance of 21.1 ± 0.1 pS (Fig. 6*C*, *Lower*; $n = 3$).

Because the appropriate characterization of the IK_{Ca} current was contingent on the use of several pharmacological compounds, we examined whether these drugs affecting IK_{Ca} channels did not cross-react with the major components of the pacemaker in hESC-CMs, the I_f and I_{NCX} currents (Fig. S4). Whereas the I_f current was highly sensitive to block by ZD7288 (25 μM), it was unaffected by KB-R7943 (3 μM), TRAM 34 (5 μM), clotrimazole (5 μM), and dequalinium (50 μM) (Fig. S4*A*). Similarly, the I_{NCX} current was insensitive to TRAM 34 (5 μM) and clotrimazole (5 μM) but was markedly depressed by KB-R7943 (3 μM) (Fig. S4*B*).

To characterize in depth the presence IK_{Ca}/SK4 channels at the mRNA and protein levels, we performed real-time PCR, Western blot, and immunocytochemistry experiments. Fig. 7*A* shows RT-PCR data from early stage-derived hESC-CMs (EBs 16 d in vitro) that demonstrate using exon-spanning primers (Table S1), the presence of transcripts of the human SK4 channel gene (KCNN4) encoding the Ca^{2+}-activated intermediate K^+ conductance (IK_{Ca}/KCa3.1). In addition, these early stage-derived hESC-CMs expressed transcripts of the voltage-gated cation channels hyperpolarization-activated cyclic nucleotide-gated ion channel (HCN)2, HCN4, voltage-gated Na^+ channel 1.5 (Nav1.5), voltage-gated Ca^+ channel 1.3 (isoform α1D) [Cav1.3 (α1D)], the Na^+/Ca^{2+} exchanger NCX1, and the homeobox transcription factor T-box protein 3 (Tbx3), which plays a pivotal role in the differ-

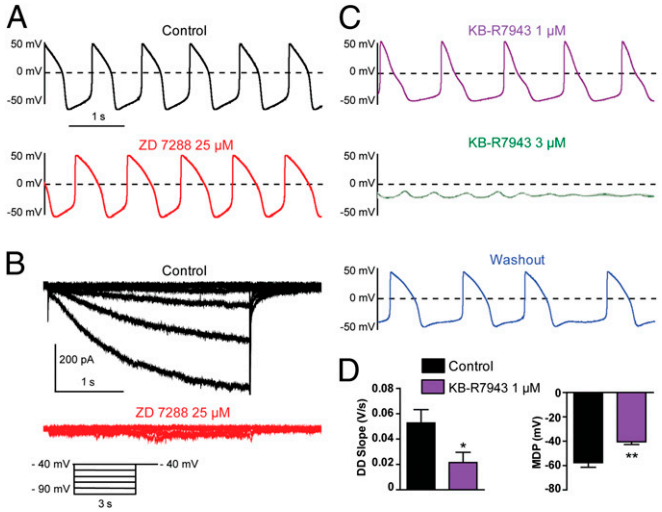

Fig. 4. A subset of hESC-CMs with prominent I_f-independent pacemaker is insensitive to ZD7288 but responsive to KB-R7943. (*A*–*C*) Combined current- and voltage-clamp recordings were performed in the same cell. (*A*, *Upper*) Spontaneous AP pattern of an hESC-CM recorded under current-clamp in control conditions. (*B*) The I_f current was subsequently recorded in the same cell, under voltage-clamp, in the absence (black traces) and presence of 25 μM ZD7288 (red traces) by stepping the membrane from a holding potential of −40 mV to −90 mV in 10-mV decrements for 3 s pulse duration. Once I_f current inhibition by ZD7288 was monitored under voltage-clamp, the AP pattern of the same cell was examined under current-clamp, during continuous ZD7288 exposure; note the lack of significant effect on pacing (see *A*, *Lower*). (*C*, *Top*) Following ZD7288 washout, the same cell was exposed to 1 μM KB-R7943 (violet trace); notice the bradycardia, the MDP depolarization, and the decreased DD slope. (*Middle*) The same cell was subsequently perfused with 3 μM KB-R7943 (green trace), leading to a rapid and complete loss of pacemaker activity. (*Bottom*) The same cell was washed out and partially recovered its pacemaker (blue trace). (*D*) KB-R7943 (1 μM) significantly decreased the DD slope (**P* = 0.0482, *n* = 6) and depolarized the MDP (***P* = 0.0091, *n* = 6) in this subset of cells.

entiation of the cardiac pacemaker tissue (1) (Fig. 7*A*). Notably, the presence of IK_{Ca} /SK4 channels could be confirmed at the protein level by Western blotting, where an immunoreactive band of about 47 kDa could be seen (Fig. 7*C*). The specificity of the anti-SK4 antibodies was verified by transfecting of HEK 293 cells with a plasmid encoding the human SK4 channel cDNA, which yielded a similar specific band pattern (Fig. 7*D*). In addition to SK4 channels, the Western blot revealed the presence of HCN2, HCN4, Nav1.5, Cav1.3 (α1D), and NCX1 proteins (Fig. 7*C*). Finally, using anti-SK4 antibodies, we found a specific immunostaining in young beating clusters (Fig. 7*E*, *Upper*), and in dissociated hESC-CMs coexpressing the cardiac α actinin and displaying a diffuse KCa3.1 immunoreactive pattern (Fig. 7*E*, *Lower*).

Expression of IK_{Ca} /SK4 Channels in Late Stage-Derived hESC-CMs and Their Impact on Pacemaker Activity. Because the pacemaker activity was sensitive to IK_{Ca} blockade in 100% of early stage-derived hESC-CMs (EBs 11–21 d in vitro), it was important to examine whether IK_{Ca} /SK4 channels were expressed in older beating EBs and if so whether they were involved in the pacemaker of their dissociated hESC-CMs. For this purpose, we isolated mRNAs from early beating clusters (EBs 15–18 d in vitro) and late stage-derived beating EBs (46-52 d in vitro) and then performed a quantitative real-time PCR (Fig. 7*B*). PCR data were quantified according to β tubulin transcript abundance and normalized to the highest abundant mRNA. The results showed that the transcript encoding SK4 channels is 3.5-fold more abundant in late stage-derived beating EBs than in early stage-derived beating clusters (Fig. 7*B*). Next, we examined, at the functional level, the sensitivity of the pacemaker to TRAM 34 blockade (5 μM) in late stage-derived beating hESC-CMs (Fig. 7 *F* and *G*). Out of 20 cells examined, 70% (*n* = 14 cells) exhibited an automaticity that was completely insensitive to TRAM 34, even at concentration as high as 20 μM (Fig. 7*F*, *Upper*). The remaining 30% of the cells (*n* = 6) showed a pacemaker activity that was highly sensitive to TRAM 34 inhibition (Fig. 7*F*, *Lower*). Remarkably, the TRAM 34-sensitive cells exhibited significantly faster beating rate and larger DD slope compared with the TRAM 34-insensitive cells (Fig. 7*G*; mean rate = 116 ± 26 bpm versus 32 ± 3 bpm and mean DD

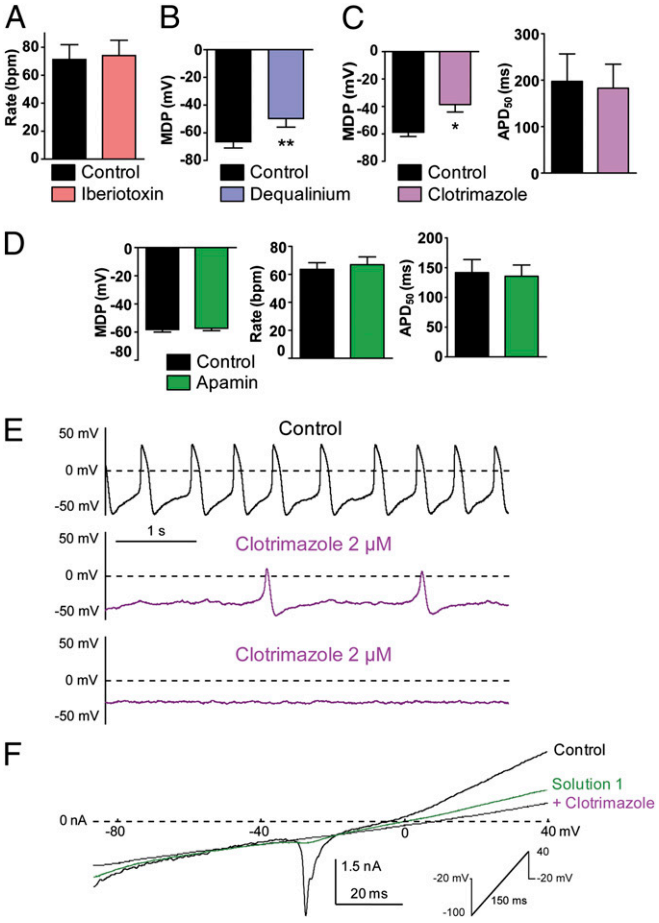

Fig. 5. Characterization of a Ca^{2+}-activated K^+ current, IK_{Ca}, and its impact on the pacemaker in early stage-derived hESC-CMs (11–21 d in vitro). (*A*) Iberiotoxin did not affect the AP beating rate (*n* = 3). (*B*) Dequalinium (50 μM) significantly depolarized the MDP (***P* = 0.0067, *n* = 5). (*C*) Clotrimazole (2 μM) significantly depolarized the MDP (**P* = 0.0135, *n* = 6) but did not affect APD_{50}. (*D*) Apamin (1 μM) did not significantly affect the MDP (*Left*), AP beating rate (*Center*) and APD_{50} (*Right*) (*n* = 5). (*E*) Spontaneous AP pattern of a hESC-CM recorded under current-clamp before (control, black trace) and following treatment with 2 μM clotrimazole (violet trace). Note the bradycardia, MDP depolarization, and the decreased DD slope. (*F*) Cells at −20 mV to cause inactivation of nearly all Na^+ channels and a substantial part of Ca^{2+} channels. Using a voltage-ramp protocol under voltage-clamp (holding at −20 mV, ramp of 150 ms from −100 to +40 mV with 1 μM free Ca^{2+} in the patch pipet solution), a clotrimazole-sensitive current could be isolated by stepwise blockade of various conductances. In the absence of blockers, the voltage ramp (black trace) revealed the presence of a voltage-dependent inward current activating at about −30 mV and corresponding to L-type Ca^{2+} currents as it was eliminated in the presence of 1 μM nifedipine (solution 1, green trace). Solution 1 contains 1 μM nifedipine, 10 μM zatebradine, and 10 μM E4031. Addition of 5 μM clotrimazole (violet trace) to solution 1 symmetrically reduced the linear current trace in both the inward and the outward directions.

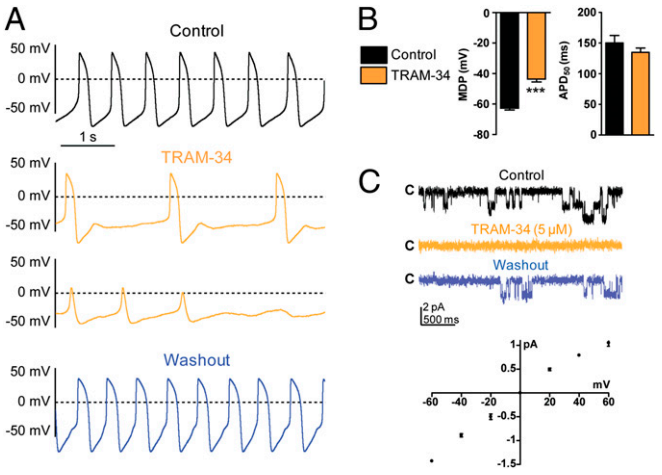

Fig. 6. Characterization of a TRAM-sensitive Ca^{2+}-activated K^+ current and its effect on the pacemaker in early stage-derived hESC-CMs (11–21 d in vitro). (*A*, *Top*) Spontaneous AP pattern of an hESC-CM recorded under current-clamp in control conditions, during continuous TRAM 34 exposure (two *Middle* panels, orange trace); note the rapid loss of pacemaker activity. The same cell was washed out (*Bottom*, blue trace). (*B*) TRAM 34 (2 μM) depolarized the MDP (***P = 3.16891E−13, n = 30) but did not affect APD_{50}. (*C*, *Upper*) Representative single channel current recorded at −60 mV from an inside-out patch containing two channels in the absence (black trace) and presence of TRAM 34 (5 μM) (orange trace) and after washout (blue trace). (*Lower*) Unitary current-voltage relations of TRAM 34-sensitive current recorded from inside-out patches and yielding upon linear regression a unitary slope conductance of 21.1 ± 0.1 pS (n = 3).

slope = 0.096 ± 0.018 versus 0.008 ± 0.002; n = 6–14, for respectively TRAM 34 sensitive and TRAM 34 insensitive cells, $P < 0.0001$).

Identification of IK_{Ca} /SK4 Channels in hESC-CMs Derived from Another Independent Human ES Cell Line, H7, and Their Impact on Pacemaker Activity. To examine the generality of the expression and function of IK_{Ca} /SK4 channels in hESC-CMs, we used another independent human ES cell line, H7 (41), to derive the cardiac cells. Fig. S11*A* shows RT-PCR data from early stage H7-derived EBs (18 d in vitro) that demonstrate, like for EBs derived from the H9.2 cell line, the presence of transcripts of the human SK4 channel gene as well as those of voltage-gated cation channels HCN2, HCN4, Nav1.5, Cav1.3 (α1D), the Na^+/Ca^{2+} exchanger NCX1, and the homeobox transcription factor Tbx3. Similar to EBs derived from the H9.2 cell line, the presence of SK4 channels as well as HCN2, HCN4, Nav1.5, Cav1.3 (α1D), and NCX1 proteins could be confirmed at the protein level by Western blotting in early stage H7-derived EBs (Fig. S11*B*). Remarkably, TRAM 34 inhibited the pacemaker activity in all tested cells of the early stage H7-derived hESC-CMs (EBs 15–18 d in vitro; Fig. S11*C*, n = 6).

Discussion

In this work, we used hESC-CMs isolated from young contracting EBs as a model to study the embryonic pacemaker mechanisms of human heart. Recording alternatively in the same cell, basal automaticity under current-clamp and ionic currents under voltage-clamp, we found that hESC-CMs are heterogeneous and exhibit three main pacemaker phenotypes, one predominantly I_f-dependent, one predominantly I_f-independent, and a combination of both. However, these phenotypes share a depolarizing drift of the MDP following treatment with blockers of the voltage clock and the Ca^{2+} clock. Our findings suggest that this MDP depolarization partly arises from inhibition of a previously unidentified Ca^{2+}-activated K^+ current found in early and late stage-derived hESC-CMs, which we characterized by patch-clamp recording, real-time PCR, Western blotting, and immunocytochemistry as belonging to KCa3.1 intermediate-conductance Ca^{2+}-activated K^+ channels (IK_{Ca}/SK4). Accordingly, IK_{Ca} inhibition leads to MDP depolarization and pacemaker suppression.

Spontaneously beating cardiomyocytes derived from human and mouse embryonic stem cells were previously described as heterogeneous (18, 19, 22, 23). In our study, hESC-CMs also showed heterogeneity when considering their APD_{50} and pacemaker phenotype. They exhibit properties more reminiscent of embryonic hearts than adult cardiac muscle, with strong pacemaker activity (mean DD slope of 0.088 V/s), very slow upstroke (mean dV/dt_{max} of 7.09 V/s), and depolarized MDP (mean MDP of −56 mV). The age of our beating hESC-CMs, obtained 11–21 d after EB formation, was younger than that of previous studies, which ranged from 20 to 95 d post-EBs (19, 22, 25). Our hESC-CMs preparation shares properties similar to those recently described in embryonic murine cardiomyocytes (E8–E9), including DD slope and upstroke values (33, 34). Exposure of these embryonic cardiomyocytes to NCX or L-type Ca^{2+} channel blockers, KB-R7943, or nifedipine, respectively, leads to fast block of automaticity, paralleled by MDP depolarization (33, 34). These features suggest that, in both hESC-CMs and murine embryonic cardiac cells, L-type Ca^{2+} channels play a crucial role in the late DD (together with NCX) and in AP upstroke (34). In addition, external Ca^{2+}-free solution or nifedipine exposure led to a fast and complete block of APs (Fig. S2). Although we detected at the mRNA and protein levels the presence of voltage-gated Na^+ channels (Nav1.5) in our young hESC-CMs preparation (EBs 11–21 d in vitro), their impact is probably very small regarding the low upstroke values and the lack of TTX effect on automaticity (Fig. S2). This feature likely results from the relatively positive resting potential in hESC-CMs (about −60 mV to −50 mV) compared with adult cardiomyocytes. Under these conditions, most of voltage-gated Na^+ channels are inactivated, which significantly reduces their contribution to AP upstroke.

Although the cardiac pacemaker was discovered more than a hundred years ago, the pacemaker mechanisms remain vigorously debated and controversial (14). We focused our study on basal automaticity and found that hESC-CMs exhibit heterogeneous pacemaker profiles. One hESC-CMs population (~32%) showed a prominent I_f-dependent pacemaker. In these cells, ZD7288 or zatebradine fully suppressed the I_f current as monitored by voltage-clamp, which led to a complete block of the pacemaker, preceded by MDP depolarization. Remarkably, the pacemaker of these very same cells was insensitive to two NCX blockers, KB-R7943 and the peptide FRCRCFa (Fig. 3). A second hESC-CMs population (~41%) exhibited a pacemaker that was virtually insensitive to the I_f blockers, zatebradine and ZD7288, despite the complete inhibition of the I_f current. In contrast, the pacemaker of these cells was highly sensitive to the two NCX blockers, KB-R7943 and FRCRCFa, thereby markedly depressing the pacemaker activity, producing MDP depolarization, until cessation of APs (Fig. 4, Figs. S5 and S6). These two pacemaker phenotypes operated in a mutually exclusive manner. A third hESC-CMs population (~26%) showed both I_f-dependent and I_f-independent pacemakers, being sensitive to both I_f and NCX blockers (Fig. S8), suggesting that both mechanisms can coexist.

Intracellular free calcium $[Ca^{2+}]_i$ beyond governing excitation–contraction coupling can also influence the shape and duration of APs through Ca^{2+}-sensitive ionic conductances, like the NCX current, the Ca^{2+}-sensitive chloride current, or Ca^{2+}-activated K^+ currents (7, 11). Recently, the three different isoforms of small-conductance Ca^{2+}-activated K^+ channels, SK1 to -3, were identified in mouse and human mature hearts (37, 42, 43). SK2 channels were found to play a crucial role in adult human and mouse atrial repolarization, especially during the late phase of the AP (37). Knockout of SK2 channels causes a delay in cardiac repolarization and leads to atrial arrhythmias (44). Overexpression of SK2

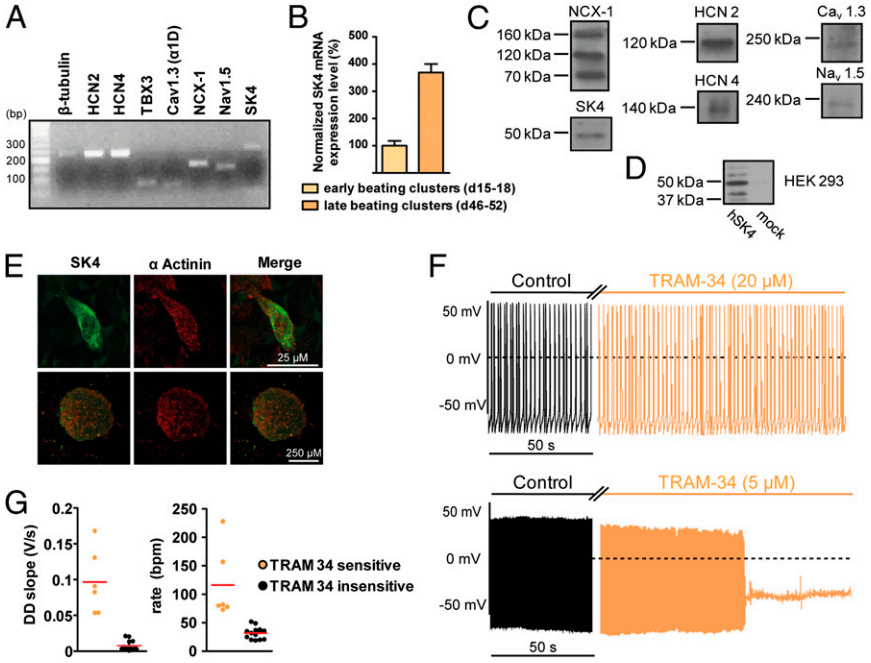

Fig. 7. Characterization of SK4 channels in early (15–18 d in vitro) and late (46–52 d in vitro) stage-derived beating EBs. (*A*) Representative agarose gel of an RT-PCR experiment performed in an early stage-derived EB (18 d in vitro) and showing bands of derived transcripts encoding β tubulin, HCN2, HCN4, Tbx3, Cav1.3 (α1D), NCX1, Nav1.5, and SK4 genes. (*B*) SK4 transcript abundance in early (15–18 d in vitro) and late (46–52 d in vitro) stage-derived beating EBs as determined by quantitative real-time PCR. Data were quantified with respect to β tubulin transcript abundance and normalized to early beating EBs transcript level (100%). $n = 3$. (*C*) Western blots showing immunoreactive bands of HCN2, HCN4, Cav1.3 (α1D), NCX1, Nav1.5, and SK4 proteins in 15-d-old beating EBs. (*D*) Western blot of lysates prepared from HEK 293 cells transfected with the hSK4 cDNA and from mock cells and probed with anti-SK4 antibodies. (*E*) Representative immunocytochemical staining using anti-SK4 and anti-α actinin antibodies in 18-d-old beating clusters (*Upper*), and in dissociated hESC-CMs (*Lower*) coexpressing the cardiac α actinin, confirming the expression of KCa3.1/SK4 channel protein. (*F*, *Upper*) Spontaneous AP pattern of a late stage-derived hESC-CM from a 52-d-old EB recorded under current-clamp before (control, black trace) and following treatment with 20 μM TRAM 34 (orange trace). Note that the pacing of this cell is insensitive to TRAM 34 even at concentrations as high as 20 μM. (Lower) Spontaneous AP pattern of another late stage-derived hESC-CM from a 52-d-old EB recorded under current-clamp before (control, black trace) and following treatment with 5 μM TRAM 34 (orange trace). Note that the beating frequency of this cell is larger than that shown in the *Upper* panel and that this hESC-CM is sensitive to TRAM 34, which leads to abrupt cessation of AP. (*G*) Data summary of late stage-derived hESC-CM (46–52 d in vitro) showing that TRAM 34-sensitive cells (orange dots) exhibited significantly faster beating rate (*Right*) and larger DD slope (*Left*) compared with the TRAM 34-insensitive cells (black dots). Mean rate = 116 ± 26 bpm versus 32 ± 3 bpm and mean DD slope = 0.096 ± 0.018 versus 0.008 ± 0.002; $n = 6$–14, for respectively TRAM 34-sensitive and TRAM 34-insensitive cells, $P < 0.0001$).

channels causes shortening of APs in atrioventricular nodal cells and an increase of their firing frequency (45).

In this study, we identified in hESC-CMs a previously unrecognized Ca^{2+}-activated K^+ conductance, which was insensitive to apamin and iberiotoxin but was fully blocked by low concentrations of clotrimazole (2-5 μM) and TRAM 34 (2-5 μM). Notably, we showed that the I_f and I_{NCX} currents were unaffected by these drugs (Fig. S4). Dequalinium also blocks this conductance at higher concentration (50 μM) than that needed to inhibit the small-conductance Ca^{2+}-activated K^+ current SK2 (39). This current was identified as an IK_{Ca} conductance not only at the whole-cell level but also at the single channel level (TRAM 34-sensitive unitary current) with a unitary slope conductance of about 21 pS, a value within the range found for intermediate conductance Ca^{2+}-activated K^+ channel family (20-80 pS) (46). The molecular identity of IK_{Ca} as KCa3.1 (SK4) channels was further confirmed at the mRNA and protein levels by PCR, Western blotting, and immunocytochemistry. All pacemaker phenotypes shared the depolarizing drift of the MDP occurring before cessation of APs, when cells were exposed to blockers of the voltage clock or the Ca^{2+} clock, suggesting that both mechanisms converge to a common pacemaker component. This MDP depolarization was previously observed in various studies performed in early embryonic mouse cardiomyocytes as well as in mouse ESC-CMs (27, 34, 47). We showed that IK_{Ca} inhibition by dequalinium, clotrimazole, or TRAM 34 leads to MDP depolarization and suppresses the pacemaker activity. Notably, IK_{Ca} inhibition did not affect APD_{50} duration (Figs. 5*C* and 6*B*), suggesting that this conductance does not play a significant role in the repolarization phase of the AP, in contrast to SK2 channels for atrial AP (37).

So, if IK_{Ca} is not involved in the repolarization of the pacemaker AP, what is its plausible role in the pacemaker and how does IK_{Ca} inhibition account for the MDP depolarization? We assume that IK_{Ca} contributes to the MDP driving force, which concurrently activates I_f and exquisitely balances inward currents of the voltage and Ca^{2+} clocks during diastolic depolarization. We posit that, during the DD of the embryonic pacemaker, there is enough intracellular free calcium $[Ca^{2+}]_i$ to activate IK_{Ca} and shape the DD by opposing the inward currents contributed by I_f and/or NCX (Fig. 8). IK_{Ca} is ideally suited for such a role because hSK4, the subunit encoding this conductance, was found to exhibit a high affinity for $[Ca^{2+}]_i$ (EC_{50} = 95 nM) compared with SK1 and SK2 channels (EC_{50} = 600–700 nM) (48). For example, in guinea-pig SAN cells, the minimum diastolic $[Ca^{2+}]_i$ concentration was found to be 225 nM, which is well enough to activate IK_{Ca} (47). The progressive decrease in $[Ca^{2+}]_i$ from early to late DD operated by the NCX-induced Ca^{2+} outflow will gradually reduce IK_{Ca} function and allow the I_f and/or I_{NCX} inward currents to take over and reach the next AP threshold. In contrast, the "non-tuned" inhibition of IK_{Ca} by dequalinium, clotrimazole, or TRAM 34 is so strong that it rapidly depolarizes the MDP and ceases the pacemaker activity by driving the Ca^{2+} channels to an inactivation state. Our results are in excellent agreement with recent studies showing that SK4 channels are critical players in cardiac pacemaker

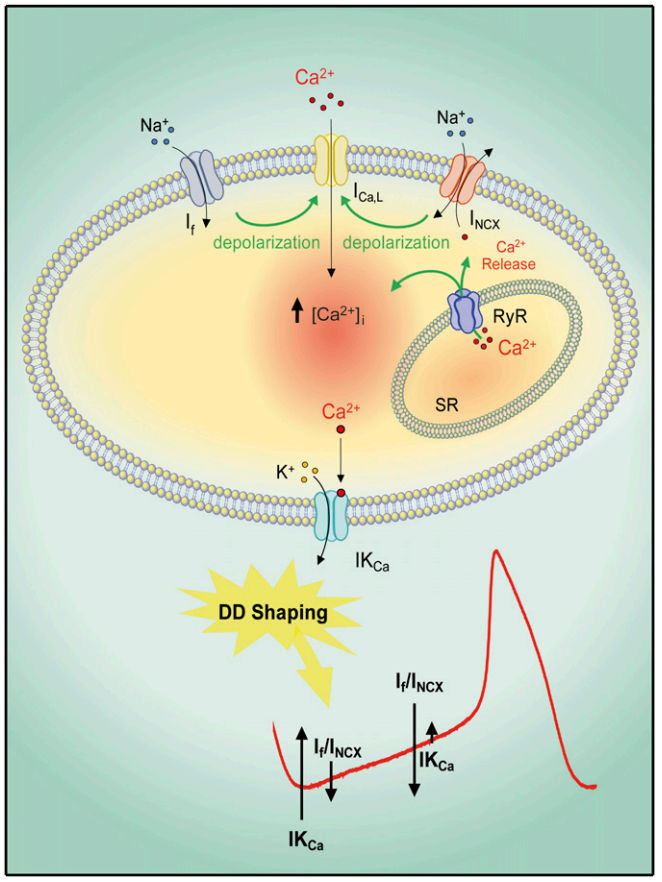

Fig. 8. Pacemaker model of human embryonic cardiomyocytes. During the early phase of DD, there is enough $[Ca^{2+}]_i$ to activate IK_{Ca}, which contributes to the MDP driving force and concurrently activates I_f. The I_f and/or the NCX currents triggered by the cyclical Ca^{2+} release from SR depolarize the membrane to activate L-type Ca^{2+} channels ($I_{Ca,L}$) and cause AP cycling. The progressive decrease in $[Ca^{2+}]_i$ from early to late DD operated by the NCX-induced Ca^{2+} outflow will gradually reduce IK_{Ca} and allow inward currents to take over and reach the next AP threshold. Thus, IK_{Ca} finely balances inward currents of the "voltage" and Ca^{2+} clocks and thereby has a crucial role in shaping the DD and the pacemaker activity.

fate determination in embryonic stem cells and induced pluripotent stem cells of mice (47, 49–51) and humans (52). Treatment with 1-ethyl-2-benzimidazolinone (EBIO), the SK4 opener of IK_{Ca}, differentiates mouse embryonic stem cells into cardiomyocytes with a strong enrichment of pacemaker-like cells (50). This differentiation was accompanied by induction of SAN-specific genes and by a loss of the ventricular-specific gene program (50). Notably, the SK4 blocker clotrimazole inhibited EBIO-induced cardiogenesis and pacemaker transcript up-regulation (50). In addition, transcriptional analysis showed a ninefold up-regulation of SK4 in the developing conduction system compared with SK1 to -3 (53). In line with this latter study, our data showed that the transcript encoding SK4 channels is 3.5-fold more abundant in late stage-derived beating EBs than in early stage-derived beating EBs (Fig. 7*B*). However, automaticity was sensitive to IK_{Ca} blockade in 100% of early stage-derived hESC-CMs but in only 30% of late stage-derived hESC-CMs. Expectedly, over time of differentiation, there is a growing number of cells beating at lower frequency and exhibiting smaller DD slope. We suggest that, during EB differentiation, SK4 channel expression is predominant in fast-beating pacemaker-like cells, which represent a smaller population compared with working cardiomyocyte-like cells. These recent studies (49, 50, 53), together with our present results, strongly suggest that KCa3.1/SK4 may be pivotal not only for selective pacemaker cell differentiation but also for pacemaker function.

Then, how does voltage clock or Ca^{2+} clock inhibition lead to MDP depolarization? We assume that I_f current blockade by ZD7288 or zatebradine leads to decreased Na^+ influx, which will stimulate the forward mode of the NCX activity and thereby enhance Ca^{2+} outflow and ultimately reduce the DD cytosolic $[Ca^{2+}]_i$. The decreased $[Ca^{2+}]_i$ will eventually shut down IK_{Ca}, which together with the enhanced NCX electrogenic activity will depolarize the MDP and cease APs (Fig. 8). Reduction in $[Ca^{2+}]_i$ and subsequent suppression of beating were recently observed in mouse embryonic (E8–E9) cardiomycytes following ZD7288 treatment (33). Similarly, we suggest that NCX blockade by KB-R7943 and FRCRCFa will decrease depolarization, subsequently reduce L-type Ca^{2+} channel activity operating at late DD, and ultimately reduce the DD cytosolic $[Ca^{2+}]_i$, thereby leading to IK_{Ca} closure, MDP depolarization, and suppression of pacemaker activity (Fig. 8). A decrease in $[Ca^{2+}]_i$ and subsequent suppression of pacemaker activity were recently described in guinea-pig SAN and mouse embryonic (E8–E9) beating cardiomyocytes following treatment with KB-R7943 (34, 47). The same final consequences (IK_{Ca} inhibition and MDP depolarization) stand for RyR inhibition by ryanodine (Fig. 8). The generality of this phenomenon was confirmed by the similar data obtained with another independent human ES cell line, H7, used to derive the hESC-CMs (Fig. S11).

In summary, we demonstrated that the voltage and Ca^{2+} clock" pacemaker mechanisms can functionally coexist in the same hESC-CM, but they can also operate in a mutually exclusive fashion in other cell populations. We found that, at the MDP, the I_{NCX} current density is higher than that of I_f. However, currently it is difficult to predict in which cell the pacemaker will be preferentially driven by I_f or by NCX or by both, when exclusively taking into account the relative current densities of I_f and NCX. It is unclear yet what governs the balance between these two mechanisms. It is possible that the density of IK_{Ca} might play a role in this fine-tuning. Future work will be needed to examine the expression and function of IK_{Ca} (KCa3.1) in vivo in the adult human cardiac nodal tissue. Importantly, this study showed that the two pacemaker clocks converge onto a diastolic component, KCa3.1 channels (IK_{Ca}, SK4), which plays a pivotal role in human embryonic cardiac automaticity by providing a driving force for the MDP and by delicately balancing the inward currents of the voltage and Ca^{2+} clocks during diastolic depolarization.

Materials and Methods

The procedures followed for experimentation and maintenance of the animals were approved by the Animal Research Ethics Committee of Tel Aviv University in accordance with Israeli law and in accordance with the Guide for the Care and Use of Laboratory Animals (1996, National Academy of Sciences, Washington, DC).

Drugs. Zatebradine, nifedipine, dequalinium chloride, and clotrimazole were purchased from Sigma; ZD7288, KB-R7943 mesylate, and TRAM 34 were purchased from Tocris; the cyclic hexapeptide FRCRCFa was synthesized; and ryanodine, tetrodotoxin (TTX), iberiotoxin, and apamin were obtained from Alomone Labs.

Quantitative Real-Time PCR. Total RNA was extracted from beating EBs of the indicated age using RNeasy microKit (Qiagen). cDNA was synthesized using Invitrogen SuperScript III RT-PCR-Kit. Real-time PCR was performed in a StepOnePlus device (Applied Biosystems), using SYBR FAST (KAPA Biosystems). The exon-spanning primers for real-time PCR are detailed in Table S1. Amplification was performed in 40 cycles of 95 °C for 3 s and 60 °C for 30 s, except for SK4 primer pair, which was 95 °C for 3 s and 65 °C for 30 s. Data were quantified with respect to β tubulin transcript abundance.

ES Culture, EB Induction, and Differentiation into hESC-CMs. Human embryonic stem cells (hESC) from the H9.2 line were grown on mitomycin C-inactivated mouse embryonic fibroblasts (MEF), with stem cell culture medium containing 80% DMEM F-12 (Biological Industries), 20% Knock Out SR (Invitrogen),

2 mM L-glutamine, 0.1 mM β-mercaptoethanol (Gibco), and 1% NEA (Gibco), supplemented with 4 ng/mL of basic Fibroblast Growth Factor (Invitrogen) to keep the cells in an undifferentiated state. The media were replaced every day, and the cells were passaged twice a week. For EBs induction (d0), ES colonies were removed from their MEF feeder by collagenase IV treatment and collected. After centrifugation, the cells were resuspended in EBs medium containing 80% DMEM (Gibco), 20% FBS (HyClone), 1% NEA, and 1 mM L-Glutamine and plated on 58-mm Petri dishes. After 7 d of culture in suspension, EBs were plated on 0.1% gelatin-coated plates and checked daily until a spontaneous beating activity was visible (generally onset of beating at day 9 after the initiation of differentiation). Beating clusters were mechanically dissected from EBs, following a three-step dissociation protocol as previously described (54). The hESC-CMs were isolated and plated on Matrigel or 0.1% fibronectin-coated glass coverslips (13 mm diameter) in 24-well plates. The coverslips were then incubated at 37 °C, and a recovery period of 2 d was given before any electrophysiological experiment was performed.

Western Blotting. Embryoid bodies (~30 EBs) were resuspended in ice-cold lysis buffer (50 mM Tris·HCl pH 7.5, 100 mM NaCl, 1% Nonidet P-40, 0.1% SDS), supplemented with protease inhibitor mixture (Sigma-Aldrich) and 1 mM phenylmethylsulfonyl fluoride (Sigma-Aldrich), and incubated on ice for 45 min, followed by vortex every 2–3 min and centrifuged for 15 min at 4 °C at 16,000 × *g*. Equal amounts of proteins (30 μg) of the resulting lysate supernatant were mixed with Laemmli sample buffer and fractionated by 12% SDS/PAGE. The resolved proteins were electro-blotted onto a nitrocellulose membrane. The membrane was incubated with the primary antibodies followed by horseradish peroxidase-conjugated secondary anti-IgG antibodies (1:10,000). The primary antibodies used were as follows: monoclonal anti-SK4/KCa3.1, 1:200 (Alomone Labs), mouse anti-NCX1, 1:200 (Thermo Scientific), rabbit anti-HCN2 1:200 (Alomone Labs), rabbit anti-HCN4 1:200 (Alomone Labs), rabbit anti-Cav1.3 1:200 (Alomone Labs), and rabbit anti-Nav1.5, 1:200 (Alomone Labs). Signals were developed using SuperSignal West Pico Chemiluminescent Substrate (Thermo Scientific).

HEK 293 Cell Transfection. HEK 293 cells were transfected with the plasmid encoding the human SK4 channel (hIK-pEGFP-C1) using the calcium phosphate method. Cells were washed in PBS and lysed in ice-cold lysis buffer. Equal amounts of proteins (30 μg) of the resulting lysate supernatant were processed for gel electrophoresis and Western blotting as above.

Immunocytochemistry. Immunocytochemistry was carried out using a post fixation technique, 2 d after a partial dissociation of the beating clusters. All primary and secondary antibodies were diluted in a blocking solution (1:50 and 1:200, respectively), consisting in Ca^{2+}- and Mg^{2+}-free PBS, 0.01% (wt/vol) BSA, and 5% (vol/vol) Calf Serum (Sigma). Briefly, hESC-CMs were first incubated for 10 min in the blocking solution, then in the presence of monoclonal anti-KCa3.1 (ALM-51, Alomone Labs) for 1 h at room temperature, followed by two washes in PBS. The cells were fixed for 10 min in 4% paraformaldehyde and rinsed twice in PBS, before and after the incubation with the secondary anti-mouse Dylight405 (KPL) antibody for 1 h in the dark. After a 5-min permeabilization with the blocking buffer containing 0.01% Triton X-100 and two PBS washes, cells were incubated for 1 h at room temperature with the polyclonal anti-α-actinin (H300 sc-15335; Santa Cruz Biotechnology). The secondary anti-rabbit Cy3 (The Jackson Laboratory) was used for the last incubation for 1 h at room temperature, followed by two washes in PBS. The coverslips were mounted on glass slides with anti-fade reagent (Gelmount; Sigma). The cells were observed with a Leica SP5 spectral scanning confocal microscope.

Electrophysiology. In all experiments, the coverslips were perfused at 33 °C with an external solution containing (in mM): 140 NaCl, 4 KCl, 11 Glucose, 1.2 $MgCl_2$, 1.8 $CaCl_2$, 5.5 Hepes titrated to pH 7.4 with NaOH and adjusted at 320 mOsm with saccharose. The whole-cell patch-clamp recordings (voltage- and current-clamp configurations) were performed with an Axopatch 200A amplifier (Molecular Devices) and pCLAMP 10.02 software (Molecular Devices). Signals were digitized at 5 kHz and filtered at 2 kHz. Microelectrodes with resistances of 4–7 MΩ were pulled from borosilicate glass capillaries (Harvard Apparatus) and filled with an intracellular solution containing (in mM): 130 KCl, 5 MgATP, 5 EGTA, 10 Hepes titrated to pH 7.3 with KOH and adjusted at 290 mOsm with saccharose. Free calcium concentrations (100 nM or 1 μM) in the intracellular solution were titrated with EGTA and $CaCl_2$ using the "EGTA calculator" software. Series resistances (5–15 MΩ) were compensated (75–90%) and periodically monitored. I_{NCX} current recording was performed with slight modifications of a previously described work (55). The extracellular solution contained (in mM): 140 NaCl, 1.8 $CaCl_2$, 1.2 $MgCl_2$, 0.001 nifedipine, 0.02 ouabain, 0.001 ryanodine, 0.01 zatebradine, 5.5 Hepes, and 11 glucose; pH was adjusted to 7.4 with NaOH. The pipette solution contained (in mM): 65 CsCl, 20 NaCl, 5.0 Na_2ATP, 1.75 $CaCl_2$, 4.0 $MgCl_2$, 10 Hepes, 20 tetraethyl ammonium chloride, and 5 EGTA (pH 7.2, adjusted with CsOH) to get 100 nM free Ca^{2+} concentration. At a holding potential of –40 mV, the currents were elicited with a ramp voltage pulse (215 ms). The test potential initially depolarized from –40 mV to +50 mV, then hyperpolarized to –100 mV, and depolarized back to –40 mV at a rate of 680 mV/s. For inside-out recording, a symmetrical high K^+ solution was used, which consisted of (in mM): 130 KCl, 10 Hepes (pH 7.3), 2 $MgCl_2$, and $CaCl_2$ and EGTA in appropriate concentrations to give a free Ca^{2+} concentration of 1μM. The free Ca^{2+} concentration in the bath solution was estimated using MaxChelator (www.stanford.edu/~cpatton/maxc.html). Signals were sampled at 10 kHz and low-pass filtered at 0.8 kHz.

Data Analysis. Maximum diastolic potential (MDP), AP amplitude (APA), AP duration at 50% of repolarization (APD_{50}), and rate and slope of diastolic depolarization (DD slope) were analyzed with the Clampfit program (pClamp 10.02; Molecular Devices). Leak subtraction was performed offline using the Clampfit software. Data were analyzed with Excel (Microsoft) and Prism 5.0 (GraphPad Software) and are expressed as mean ± SEM. Statistical analysis was performed using the two-tailed paired Student *t* test and the linear regression for correlation and one way ANOVA followed by Tukey's Multiple Comparison Test. *P* values of less than 0.05 were assumed significant.

ACKNOWLEDGMENTS. Prof. Heike Wulff is acknowledged for her kind gift of the human SK4 plasmid. This work is supported by the Deutsch-Israelische Projektkooperation DIP fund (Deutsche Forschungsgemeinschaft), the Israel Science Foundation (ISF 488/09), and the Ministry of Health (MOH:3-6273) (to B.A.), by the Israel Science Foundation (O.B.), by the Ministry of Health-Chief Scientist (O.B.), by The Rappaport Family Institute for Research in the Medical Sciences (O.B.), by The Sohnis and Forman Families Stem Cells Center (O.B. and J.I.-E.), and by Israeli Ministry of Health Grant 2010-3-6266, USA–Israeli Binational Research Grant 2009-334, and Israel Science Foundation Grant 23/10 (to D.K.).

1. Christoffels VM, Smits GJ, Kispert A, Moorman AF (2010) Development of the pacemaker tissues of the heart. *Circ Res* 106(2):240–254.
2. Mangoni ME, Nargeot J (2008) Genesis and regulation of the heart automaticity. *Physiol Rev* 88(3):919–982.
3. Brown HF (1982) Electrophysiology of the sinoatrial node. *Physiol Rev* 62(2):505–530.
4. DiFrancesco D (1993) Pacemaker mechanisms in cardiac tissue. *Annu Rev Physiol* 55: 455–472.
5. Guo J, Mitsuiye T, Noma A (1997) The sustained inward current in sino-atrial node cells of guinea-pig heart. *Pflugers Arch* 433(4):390–396.
6. Hagiwara N, Irisawa H, Kasanuki H, Hosoda S (1992) Background current in sino-atrial node cells of the rabbit heart. *J Physiol* 448:53–72.
7. Hüser J, Blatter LA, Lipsius SL (2000) Intracellular Ca2+ release contributes to automaticity in cat atrial pacemaker cells. *J Physiol* 524(Pt 2):415–422.
8. Sanguinetti MC, Jurkiewicz NK (1990) Two components of cardiac delayed rectifier K+ current. Differential sensitivity to block by class III antiarrhythmic agents. *J Gen Physiol* 96(1):195–215.
9. Seyama I (1976) Characteristics of the rectifying properties of the sino-atrial node cell of the rabbit. *J Physiol* 255(2):379–397.
10. Shibasaki T (1987) Conductance and kinetics of delayed rectifier potassium channels in nodal cells of the rabbit heart. *J Physiol* 387:227–250.
11. Vinogradova TM, Bogdanov KY, Lakatta EG (2002) Beta-Adrenergic stimulation modulates ryanodine receptor Ca(2+) release during diastolic depolarization to accelerate pacemaker activity in rabbit sinoatrial nodal cells. *Circ Res* 90(1):73–79.
12. DiFrancesco D (2010) The role of the funny current in pacemaker activity. *Circ Res* 106(3):434–446.
13. Gao Z, et al. (2010) I(f) and SR Ca(2+) release both contribute to pacemaker activity in canine sinoatrial node cells. *J Mol Cell Cardiol* 49(1):33–40.
14. Lakatta EG, DiFrancesco D (2009) What keeps us ticking: A funny current, a calcium clock, or both? *J Mol Cell Cardiol* 47(2):157–170.
15. Lakatta EG, Maltsev VA, Vinogradova TM (2010) A coupled SYSTEM of intracellular Ca2+ clocks and surface membrane voltage clocks controls the timekeeping mechanism of the heart's pacemaker. *Circ Res* 106(4):659–673.
16. Barbuti A, et al. (2009) Molecular composition and functional properties of f-channels in murine embryonic stem cell-derived pacemaker cells. *J Mol Cell Cardiol* 46(3):343–351.
17. Dolnikov K, et al. (2006) Functional properties of human embryonic stem cell-derived cardiomyocytes: Intracellular Ca2+ handling and the role of sarcoplasmic reticulum in the contraction. *Stem Cells* 24(2):236–245.
18. Fu JD, et al. (2010) Na+/Ca2+ exchanger is a determinant of excitation-contraction coupling in human embryonic stem cell-derived ventricular cardiomyocytes. *Stem Cells Dev* 19(6):773–782.

19. He JQ, Ma Y, Lee Y, Thomson JA, Kamp TJ (2003) Human embryonic stem cells develop into multiple types of cardiac myocytes: Action potential characterization. *Circ Res* 93(1):32–39.
20. Jiang P, et al. (2010) Electrophysiological properties of human induced pluripotent stem cells. *Am J Physiol Cell Physiol* 298(3):C486–C495.
21. Méry A, et al. (2005) Initiation of embryonic cardiac pacemaker activity by inositol 1,4,5-trisphosphate-dependent calcium signaling. *Mol Biol Cell* 16(5):2414–2423.
22. Pekkanen-Mattila M, et al. (2010) Human embryonic stem cell-derived cardiomyocytes: Demonstration of a portion of cardiac cells with fairly mature electrical phenotype. *Exp Biol Med (Maywood)* 235(4):522–530.
23. Qu Y, Whitaker GM, Hove-Madsen L, Tibbits GF, Accili EA (2008) Hyperpolarization-activated cyclic nucleotide-modulated 'HCN' channels confer regular and faster rhythmicity to beating mouse embryonic stem cells. *J Physiol* 586(3):701–716.
24. Sartiani L, et al. (2007) Developmental changes in cardiomyocytes differentiated from human embryonic stem cells: A molecular and electrophysiological approach. *Stem Cells* 25(5):1136–1144.
25. Satin J, et al. (2004) Mechanism of spontaneous excitability in human embryonic stem cell derived cardiomyocytes. *J Physiol* 559(Pt 2):479–496.
26. Wang K, et al. (2005) Electrophysiological properties of pluripotent human and mouse embryonic stem cells. *Stem Cells* 23(10):1526–1534.
27. Zahanich I, et al. (2011) Rhythmic beating of stem cell-derived cardiac cells requires dynamic coupling of electrophysiology and Ca cycling. *J Mol Cell Cardiol* 50(1):66–76.
28. Hobai IA, Khananshvili D, Levi AJ (1997) The peptide "FRCRCFa", dialysed intracellularly, inhibits the Na/Ca exchange in rabbit ventricular myocytes with high affinity. *Pflugers Arch* 433(4):455–463.
29. Iwamoto T, Watano T, Shigekawa M (1996) A novel isothiourea derivative selectively inhibits the reverse mode of Na+/Ca2+ exchange in cells expressing NCX1. *J Biol Chem* 271(37):22391–22397.
30. Li L, Kimura J (2002) Effect of KB-R7943 on oscillatory Na+/Ca2+ exchange current in guinea pig ventricular myocytes. *Ann N Y Acad Sci* 976:539–542.
31. Alvarez J, Montero M, Garcia-Sancho J (1992) High affinity inhibition of Ca(2+)-dependent K+ channels by cytochrome P-450 inhibitors. *J Biol Chem* 267(17):11789–11793.
32. Brugnara C, et al. (1995) Oral administration of clotrimazole and blockade of human erythrocyte Ca(++)-activated K+ channel: The imidazole ring is not required for inhibitory activity. *J Pharmacol Exp Ther* 273(1):266–272.
33. Chen F, et al. (2010) Atrioventricular conduction and arrhythmias at the initiation of beating in embryonic mouse hearts. *Dev Dyn* 239(7):1941–1949.
34. Liang H, et al. (2010) Electrophysiological basis of the first heart beats. *Cell Physiol Biochem* 25(6):561–570.
35. Li J, Qu J, Nathan RD (1997) Ionic basis of ryanodine's negative chronotropic effect on pacemaker cells isolated from the sinoatrial node. *Am J Physiol* 273(5 Pt 2): H2481–H2489.
36. Rubenstein DS, Lipsius SL (1989) Mechanisms of automaticity in subsidiary pacemakers from cat right atrium. *Circ Res* 64(4):648–657.
37. Xu Y, et al. (2003) Molecular identification and functional roles of a Ca(2+)-activated K+ channel in human and mouse hearts. *J Biol Chem* 278(49):49085–49094.
38. Imlach WL, Finch SC, Miller JH, Meredith AL, Dalziel JE (2010) A role for BK channels in heart rate regulation in rodents. *PLoS ONE* 5(1):e8698.
39. Malik-Hall M, Ganellin CR, Galanakis D, Jenkinson DH (2000) Compounds that block both intermediate-conductance (IK(Ca)) and small-conductance (SK(Ca)) calcium-activated potassium channels. *Br J Pharmacol* 129(7):1431–1438.
40. Wulff H, et al. (2000) Design of a potent and selective inhibitor of the intermediate-conductance Ca2+-activated K+ channel, IKCa1: A potential immunosuppressant. *Proc Natl Acad Sci USA* 97(14):8151–8156.
41. Thomson JA, et al. (1998) Embryonic stem cell lines derived from human blastocysts. *Science* 282(5391):1145–1147.
42. Tuteja D, et al. (2010) Cardiac small conductance Ca2+-activated K+ channel subunits form heteromultimers via the coiled-coil domains in the C termini of the channels. *Circ Res* 107(7):851–859.
43. Tuteja D, et al. (2005) Differential expression of small-conductance Ca2+-activated K+ channels SK1, SK2, and SK3 in mouse atrial and ventricular myocytes. *Am J Physiol Heart Circ Physiol* 289(6):H2714–H2723.
44. Li N, et al. (2009) Ablation of a Ca2+-activated K+ channel (SK2 channel) results in action potential prolongation in atrial myocytes and atrial fibrillation. *J Physiol* 587(Pt 5):1087–1100.
45. Zhang Q, et al. (2008) Functional roles of a Ca2+-activated K+ channel in atrioventricular nodes. *Circ Res* 102(4):465–471.
46. Vergara C, Latorre R, Marrion NV, Adelman JP (1998) Calcium-activated potassium channels. *Curr Opin Neurobiol* 8(3):321–329.
47. Sanders L, Rakovic S, Lowe M, Mattick PA, Terrar DA (2006) Fundamental importance of Na+-Ca2+ exchange for the pacemaking mechanism in guinea-pig sino-atrial node. *J Physiol* 571(Pt 3):639–649.
48. Joiner WJ, Wang LY, Tang MD, Kaczmarek LK (1997) hSK4, a member of a novel subfamily of calcium-activated potassium channels. *Proc Natl Acad Sci USA* 94(20): 11013–11018.
49. Kleger A, Liebau S (2011) Calcium-activated potassium channels, cardiogenesis of pluripotent stem cells, and enrichment of pacemaker-like cells. *Trends Cardiovasc Med* 21(3):74–83.
50. Kleger A, et al. (2010) Modulation of calcium-activated potassium channels induces cardiogenesis of pluripotent stem cells and enrichment of pacemaker-like cells. *Circulation* 122(18):1823–1836.
51. Liebau S, et al. (2011) An inducible expression system of the calcium-activated potassium channel 4 to study the differential impact on embryonic stem cells. *Stem Cells Int* 2011:456815.
52. Müller M, et al. (2012) Ca2+ activated K channels-new tools to induce cardiac commitment from pluripotent stem cells in mice and men. *Stem Cell Rev* 8(3):720–740.
53. Horsthuis T, et al. (2009) Gene expression profiling of the forming atrioventricular node using a novel tbx3-based node-specific transgenic reporter. *Circ Res* 105(1): 61–69.
54. Mummery C, et al. (2007) Cardiomyocytes from human and mouse embryonic stem cells. *Methods Mol Med* 140:249–272.
55. Miura Y, Kimura J (1989) Sodium-calcium exchange current. Dependence on internal Ca and Na and competitive binding of external Na and Ca. *J Gen Physiol* 93(6): 1129–1145.